catalysts

MDPI

Article

Preparation of Quasi-MIL-101(Cr) Loaded Ceria Catalysts for the Selective Catalytic Reduction of NO_x at Low Temperature

Min Lu [1], Haili Hou [1], Chuanying Wei [1], Xiaohui Guan [1], Wei Wei [2,*] and Guang-Sheng Wang [3,*]

1 School of Chemical Engineering, Northeast Electric Power University, Jilin 132000, China; lumin19770919@163.com (M.L.); h18704329087@163.com (H.H.); w13844204685@126.com (C.W.); guanxh@neepu.edu.cn (X.G.)
2 School of Chemistry and Chemical Engineering, Henan Engineering Center of New Energy Battery Materials, Henan Key Laboratory of Bimolecular Reorganization and Sensing, Shangqiu Normal University, Shangqiu 476000, China
3 School of Chemistry, Beihang University, Beijing 100191, China
* Correspondence: weiweizzuli@163.com (W.W.); wanggsh@buaa.edu.cn (G.-S.W.); Tel.: +86-188-1027-1510 (G.-S.W.)

Received: 1 December 2019; Accepted: 15 January 2020; Published: 20 January 2020

Abstract: At present, the development of novel catalysts with high activity Selective Catalytic Reduction (SCR) reaction at the low temperature is still a challenge. In this work, the authors prepare CeO_2/quasi-MIL-101 catalysts with various amounts of deposited ceria by a double-solvent method, which are characterized by X-ray diffraction (XRD), Fourier Transform infrared spectroscopy (FT-IR), transmission electron microscopy (TEM), X-ray photoelectron spectroscopy (XPS), and so on. The results show that the increase of Ce content has a great influence on the catalytic property of the catalyst. The introduction of Ce can promote the conversion between Cr^{3+} and Cr^{5+} and increase the proportion of lattice oxygen, which improves the activity of the catalyst. However, the catalyst will be peroxidized when the content of Ce is too high, resulting in the decline of the catalytic activity. This experiment indicates that CeO_2/quasi-MIL-101 plays a significant role in the NH_3-SCR process at the low temperature when the loading of Ce is 0.5%. This work has proved the potential of this kind of material in NH_3-SCR process at the low temperature, providing help for subsequent studies.

Keywords: selective catalytic reduction; CeO_2/quasi-MIL-101(Cr); low temperature; metal-organic framework

1. Introduction

With the acceleration of urbanization and industrialization, people enjoy a convenient life while also suffering bad effects from various harmful pollutants. The emission control of nitrogen oxides (NO_x) resulting from fossil fuel combustion has been a major environmental concern related to air quality, as they cause a variety of environmentally harmful effects such as acid rain, photochemical smog, greenhouse effects, and ozone depletion [1–3]. At present, several methods have been used for the elimination of NO_x, such as plasma catalysis [4,5], selective catalytic reduction (SCR) [6–9], and selective non-catalytic reduction (SNCR) [10,11]. Therein, selective catalytic reduction of NO_x with NH_3 as a reductant is one of the effective techniques to remove NO_x and has been commercialized in the post-treatment of flue gases of power plants. Catalyst plays an important part in the NH_3-SCR technology. The common commercialized industrial catalysts for this process are the mixture of V_2O_5 with WO_3 and MoO_3, supported by anatase TiO_2 [12–14], which shows high catalytic activity for NO

reduction within a temperature window ranging from 300 °C to 400 °C. However, there are still some problems caused by this catalyst. For example, the catalyst is placed upstream of the electrostatic precipitator and desulfurization devices, where the flue gas needs to be reheated, and the catalyst easily suffers from the poisoning and deactivates [15–17]. Therefore, the tendency is to develop novel catalysts without vanadium at low temperatures (<300 °C) that work downstream of the electrostatic precipitator and desulfurization devices for flue gases without reheating.

In heterogeneous catalysts, most of the catalysts consist of three components: active component, cocatalysts, and carriers. The active component has a crucial influence on the catalytic activity of the catalyst, and the cocatalyst can significantly improve the activity of the catalyst as well as its selectivity. For the catalyst, the carrier is mainly to support, disperse, and stabilize the catalytically active substance. Recently, for industrial application, active catalysts are usually supported by different carriers, such as Al_2O_3 [18,19], TiO_2 [15,20], SiO_2 [21,22], ZrO_2 [6], activated carbon [23,24] and zeolites [25,26]. Although these carriers have the function of large specific surface area and supporting and stabilizing active components, the integration of high content active components and large specific surface area has become the direction of future development.

Metal-Organic Frameworks (MOFs), also known as Porous Coordination Polymers (PCPs), constructed by inorganic metal ions and metal clusters with organic linkers, have emerged as a new class of porous materials [27–29]. MOFs play a crucial role in gas storage and separation [30,31], sensing [32,33], and catalysis [34,35], which are attributed to the material having an infinite topology, high porosity, large specific surface area and highly metal content [36,37].

Among them, MILs materials are the most typical representatives. MILs are composed of a trivalent metal ion, such as Cr^{3+}, Fe^{3+}, or Al^{3+} and a carboxylic acid, such as terephthalic acid or trimesic acid [38–41]. Wang P [42] and co-workers prepared the MIL-100(Fe) catalytic materials for the SCR of NO_x with NH_3, which proved the feasibility of MOFs as a new catalyst in NH_3-SCR, and found that its excellent catalytic activity is attributed to high metal content, large specific surface area, and abundant active sites of MILs. Zhang M [43] et al. used in situ deposition to prepare Mn-based catalysts on a UiO-66 carrier for the selective catalytic reduction of NO by NH_3 (NH_3-SCR). At the same time, some scholars reported that the MOFs of the transition metal center are directly used for SCR [44–46]. In the pores of MOFs, even those with coordinatively unsaturated sites, the inorganic nodes are partitioned from the guest metal oxides or nanoparticles (NPs) by organic ligands, resulting in weak interactions between MOFs and the immobilized metal NPs. Furthermore, Tsumori N [47] et al. reported a quasi-MOF. By calcining the already prepared MIL-101(Cr), an open framework structure could be formed to expose inorganic nodes, which would contribute to the interaction between metal nanoparticles and inorganic nodes and improve the catalytic activity. Therefore, this method will be capable of achieving active ingredient-carrier integration easily.

In recent years, as a relatively nontoxic material, ceria (CeO_2) has attracted tremendous attention for its application in NH_3-SCR catalysts due to promoting the oxidization of NO to NO_2. The main reason is that it has two stable oxidation states, which are Ce^{4+} and Ce^{3+}. Meanwhile, the shift between Ce^{4+} and Ce^{3+} leads to the storage and release of oxygen, the material possesses unique redox performance and oxygen storage capacity [48,49]. Qiu et al. [50] develope cobalt and cerium doped Mn/TiO_2 catalysts, and the catalytic rate is as high as 99% at 150 °C. Boningari] and colleagues [51] report that Ce-doped Mn/TiO_2 catalysts enhance catalytic activity at low-temperature for SCR. Zhang [52] investigate the catalytic materials for the oxidation of NO using chromium-ceria doped on TiO_2-pillared clay nanocomposites catalysts, and the results indicated that the addition of CeO_x improves the oxidation to NO in the extent. Ceria, as a cocatalyst, has a significant influence on enhancing catalytic activity.

In this study, the authors investigated the feasibility of catalytic materials for the SCR of NO_x with NH_3 using the ceria as a cocatalyst doped into MIL-101(Cr) with quasi-MOF structure and explored the performance of quasi-MIL-101(Cr). The physical structure and chemical properties of the catalyst are characterized by powder X-ray diffraction (XRD), Fourier Transform infrared spectroscopy (FT-IR),

The Brunauer–Emmett–Teller (BET), Scanning electron microscope (SEM), Transmission electron microscopy (TEM), Thermogravimetric (TG), X-ray photoelectron spectroscopy (XPS), and so on.

2. Results and Discussion

2.1. Characteristics of the Catalysts

The thermal stability of MIL-101(Cr) is studied by the thermogravimetric analysis from 37 °C to 600 °C in air, and the results are shown in Figure 1. The material weight reduces by 5.6% below 200 °C in stage a, which results from the removal of physically and chemically adsorbed water at low temperatures. The loss observed at 200–300 °C is 13% in stage b, which indicated the removal of some hydroxyl groups and guest groups. In stage c (T > 300 °C), the loss of the weight increases, which indicates that the MIL-101(Cr) structure collapses, and the crystal form changes. Hence, the quasi-MIL-101(Cr) is the deligandation of the MIL-101(Cr), and this thermal stability could ensure the applicability of the catalyst over this temperature range in SCR. Figure S1 displays the thermogravimetric analysis of xCeO_2/quasi-MIL-101 doped with different ceria content. It can be seen from the figure that the trend of the three samples is similar, and they restructured after 300 °C.

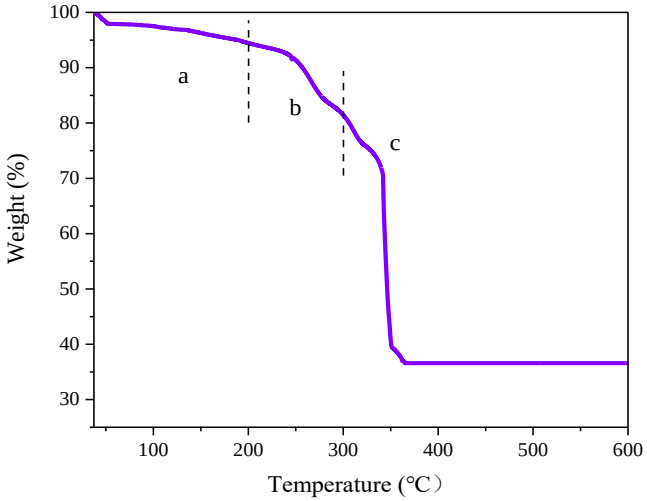

Figure 1. Thermogravimetric analysis under air (5 °C/min heated rate) of MIL-101(Cr).

The diffraction peaks of MIL-101(Cr) are consistent with the published literature [53], as shown in Figure S2. XRD patterns of the quasi-MIL-101(Cr) and CeO_2/quasi-MIL-101 catalysts with various amounts of deposited ceria being displayed in Figure 2. The quasi-MIL-101(Cr), broadening of the diffractions around 3–10° from MIL-101(Cr), is observed, which implies the partial deligandation of MIL-101(Cr) and carbon generation [47]. Due to the less Ce content, the XRD diffraction peak is not obvious [52,54]. However, ceria has a strong oxidation property. Under the same temperature of calcination, the oxidation rate of MIL-101(Cr) is enhanced, and more active sites are exposed. In addition, FT-IR spectroscopy of various samples is shown in Figure 3. FT-IR spectra of quasi-MIL-101(Cr) is almost the same as that of MIL-101(Cr). However, when the calcination temperature increases to 300 °C, the bands of carboxylates at 1630–1396 cm^{-1} broaden while the band of Cr-O at around 594 cm^{-1} indicates a red shift, which implies the partial deligandation of MIL-101(Cr). Moreover, a new broad band appears at 750–500 cm^{-1}, belonging to Cr_2O_3 and CeO_2. The original Cr-O bond disappearance may be due to the addition of Ce, which increases the oxidation performance of the catalyst. At the same temperature, partial deligandation phenomenon is aggravated, and the Cr-O bond is converted into Cr_2O_3 [47]. This is consistent with the XRD characterization.

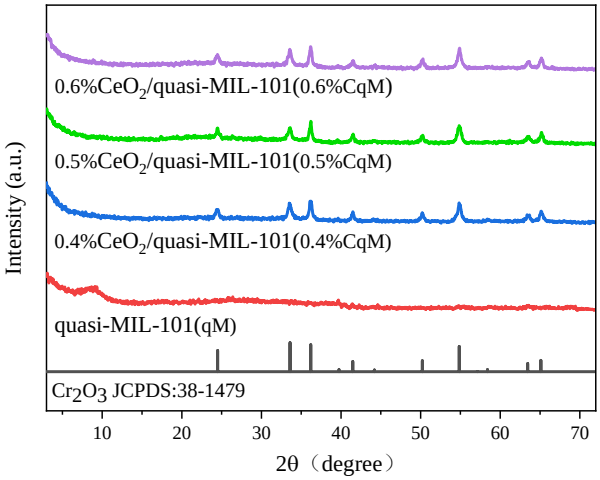

Figure 2. X-ray diffraction patterns of various catalysts.

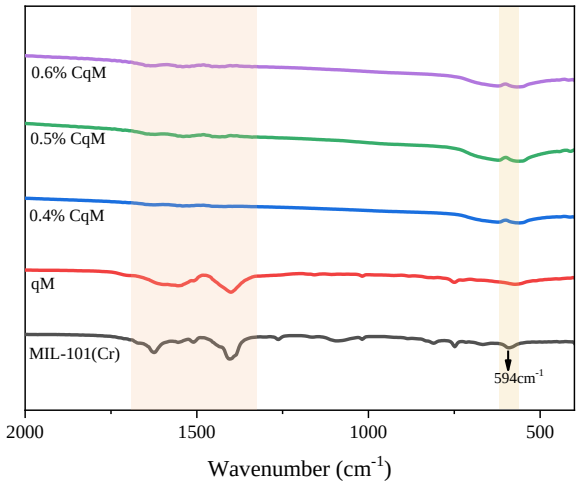

Figure 3. Fourier Transform infrared spectroscopy (FT-IR) characterization of various catalysts.

Figure S3 shows the nitrogen adsorption-desorption isotherms of MIL-101(Cr), quasi-MIL-101(Cr), and $xCeO_2$/quasi-MIL samples. Apparently, we obtained MIL-101(Cr) and quasi-MIL-101(Cr) as a type I isotherm, which indicates that pore sizes mainly distribute in microporous magnitude. In addition, Figure 4a–c displays the N_2 adsorption-desorption isotherms of $xCeO_2$/quasi-MIL-101 doped with different ceria content, respectively. They correspond to typical IV isotherms, as classified by International Union of Pure and Applied Chemistry (IUPAC), indicating the presence of mesopores [55,56]. The changing of material pore structure from microporous to mesoporous is reflected in the transformation of the isotherm type. In Figure 4a–c, it can be observed that both $xCeO_2$/quasi-MIL-101materials have H4 type hysteretic loops, indicating that the material has a mixed microporous and mesoporous pore structure. Figure 4d shows the pore size distribution of $xCeO_2$/quasi-MIL-101, corresponding to the above data. The Brunauer–Emmett–Teller (BET) surface areas of the MIL-101(Cr), quasi-MIL-101(Cr), and $xCeO_2$/quasi-MIL-101 materials with various amounts of deposited ceria are shown in Table 1. The results display that the MIL-101(Cr) sample has a BET specific area of 1767 m^2/g, the quasi-MIL-101(Cr) sample has a BET specific area of 1147 m^2/g. The decrease of specific surface areas results from the partial deligandation of the MIL-101(Cr) material by calcining at 300 °C. Furthermore, with the increase of cerium oxide content, the surface area of the prepared CeO_2/quasi-MIL-101(Cr) catalyst decreases rapidly. When the ceria content is 0.6%, the specific surface areas decreases to 203 m^2/g. We have considered that the addition of Ce may cause the blockage of pores in the materials, and the blockage of pore in materials with low Ce

content must exist, but it is not the main reason for the obvious change of the specific surface area of materials. The main reason is that Ce has strong oxidation properties. With the increase of Ce content, the peroxidization of the material results in the change of the skeleton and the decrease of the specific surface area. This is consistent with the Transmission electron microscopy (TEM) characterization (Figure S5).

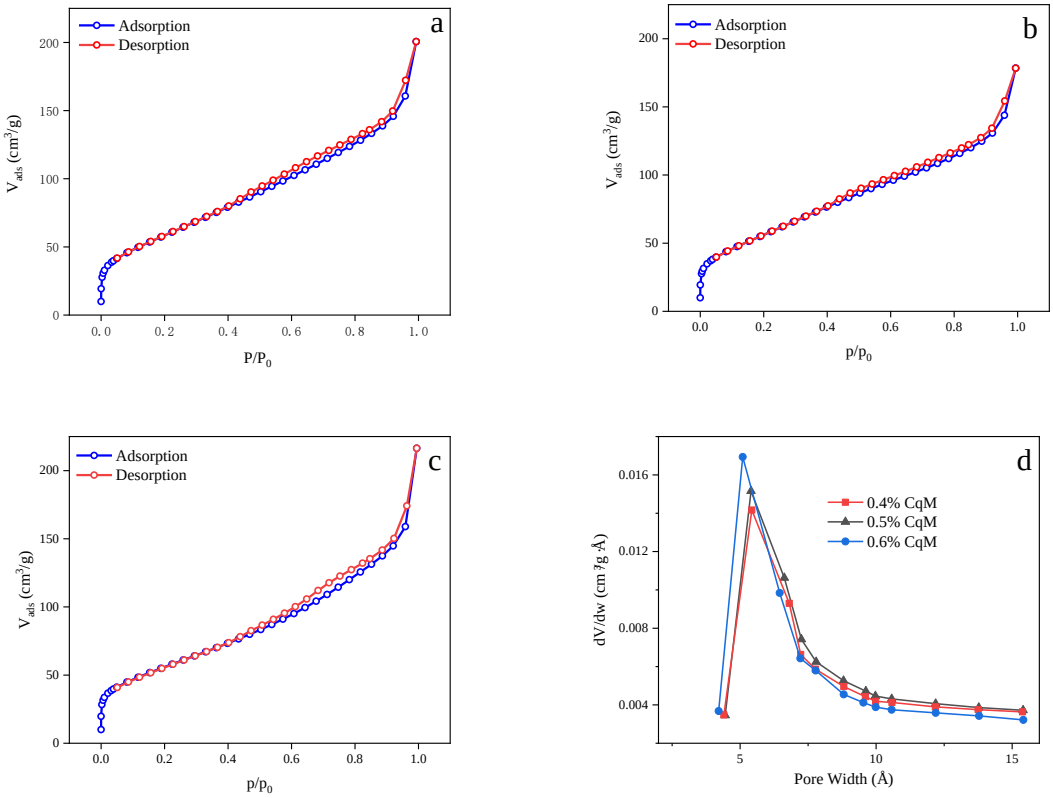

Figure 4. $xCeO_2$/quasi-MIL-101 N_2 adsorption-desorption isotherms and pore size distribution (**a**). 0.4%CeO_2/quasi-MIL-101; (**b**) 0.5%CeO_2/quasi-MIL-101; (**c**) 0.6%CeO_2/quasi-MIL-101; (**d**) Median pore width distribution of $xCeO_2$/quasi-MIL-101).

Table 1. Ce content and BET surface area over various catalysts.

Sample	Ce [1] (wt%)	S_{BET} (m^2g^1)	Median Pore Width(Å)
MIL-101(Cr)	—	1767	6.726
quasi-MIL-101(Cr)	—	1146	6.225
0.4%CeO_2/quasi-MIL-101	0.4	218	6.508
0.5%CeO_2/quasi-MIL-101	0.5	211	6.506
0.6%CeO_2/quasi-MIL-101	0.6	202	6.088

[1] Ce content was detected by the Inductive Coupled Plasma Emission Spectrometer (ICP) method.

The SEM image of the MIL-101(Cr) is shown in Figure S4. The SEM pattern indicates that MIL-101(Cr) has an octahedral crystal structure. The TEM patterns of $xCeO_2$/quasi-MIL-101 with various amounts of deposited ceria are displayed in Figure S5. According to the TEM images, it can be observed that the appearance of $xCeO_2$/quasi-MIL-101 catalysts with different Ce content still has a regular octahedral structure. However, with the increase of the Ce content, it can be observed that the skeleton of the catalysts becomes to collapse, which is attributed to the strong oxidation property of Ce. At the same calcination temperature, the addition of Ce accelerates the oxidation of the catalyst and changes its skeleton. The TEM image of the 0.5%CeO_2/quasi-MIL-101 is shown in Figure 5a. To reveal the elemental distribution on the 0.5%CeO_2/quasi-MIL-101, High-angle annular dark field

image-scanning transmission electron microscopy (HAADF STEM) image and EDS elemental mapping are performed, and the results are presented in Figure 5b–d. Figure 5b shows the HAADF STEM image of a single 0.5%CeO_2/quasi-MIL-101. The EDS elemental mappings (Figure 5c,d) demonstrate the distributions of the Cr and Ce. Due to the strong oxidation ability of Ce, the surface of the original structure is rough and overlapped with the loaded Ce, which will affect the observation of Ce. Through Figure 5c, there are still some carbon skeletons and a large number of Cr elements, which is consistent with the previously reported literature [47]. Figure 5d shows that Ce is mainly dispersed in the framework, which is attributed to the preparation of the double solvent method [57].

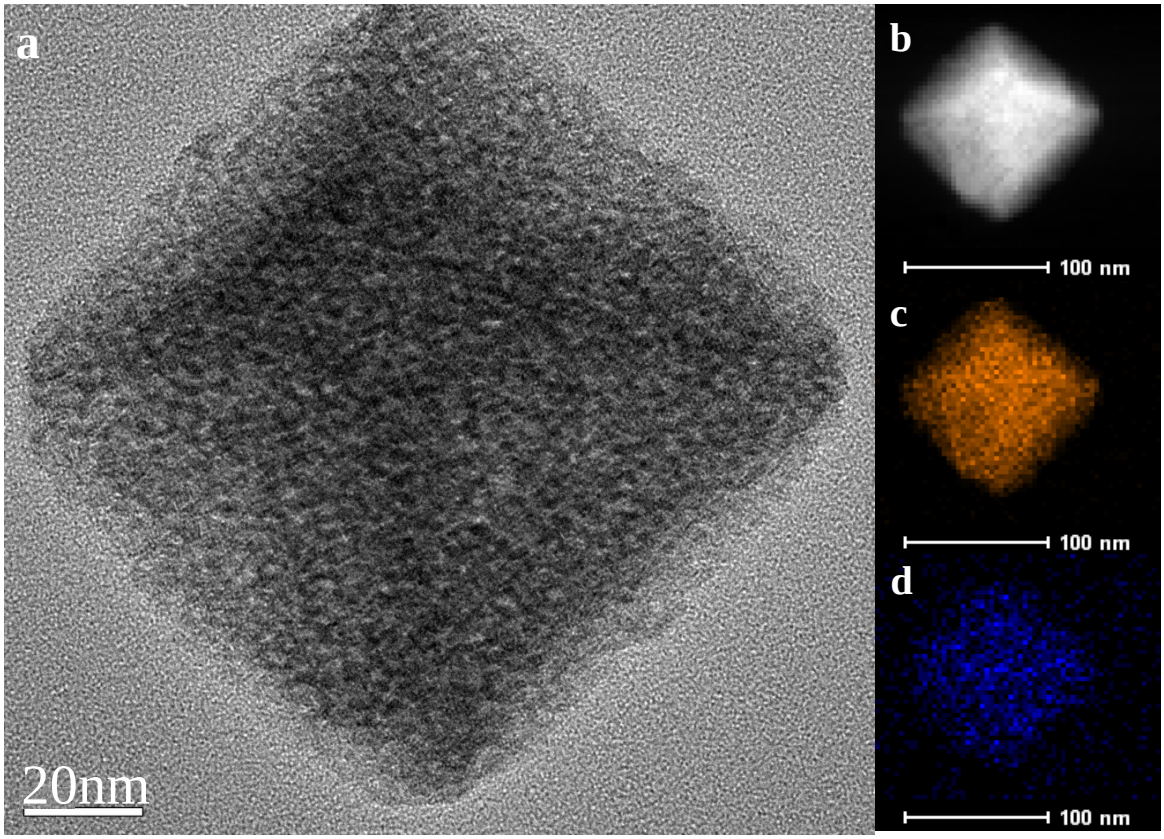

Figure 5. (**a**) TEM image of 0.5%CeO_2/quasi-MIL-101 (**b**) High-angle annular dark-field scanning transmission electron microscopy image of 0.5%CeO_2/quasi-MIL-101, and the corresponding elemental mapping images of (**c**) chromium, (**d**) cerium.

To investigate the surface chemical state of the most active catalyst, the XPS spectra of the Cr 2p and O 1s in catalysts with various amounts of deposited ceria are obtained, as shown in Figure 6. The Cr 2p of xCqM catalyst was separated into two types of peaks by the same peak-fitting deconvolution technique. The "low valence" Cr is characterized by average binding energy at about 576 eV, and the "high valence" Cr is characterized by average binding energy at about 578.3–578.5 eV [16]. The former peaks can be assigned to Cr^{2+} (575.7–576.0 eV) and Cr^{3+} (576.8–577.1 eV). The rear peak should be assigned to a higher valence chromium state at about (578.3–578.5 eV), perhaps Cr^{5+} or Cr^{6+}. Russo N [58] and his colleagues have reported that the binding energy of Cr^{5+} has a value in the range of 578.0–578.8 eV. Hence, the peaks with higher valence Cr in the range of 578.48–578.58 eV could be assigned to Cr^{5+} (Figure 6A). It has been reported that Cr^{6+} exhibits higher binding energy at about 579–580 eV, which we do not observe. It can be seen from Figure 6A that Cr^{5+} exerts a significant impact on the SCR process, which is consistent with previous literature reports. Table 2 lists the binding energies of core electrons of xCqM and the percent of differential valence state. Due to the low content of ceria, XPS cannot be clearly observed. However, with the addition of the Ce element, the proportion

of Cr^{3+} decreases, and that of Cr^{5+} rises. It indicates that the Cr has the oxidation reaction, and the binding energy is shifted toward the high energy direction, which is caused by the addition of the Ce element. Meanwhile, the addition of Ce accelerates the conversion between Cr^{3+} and Cr^{5+}, improving the redox performance of the catalyst.

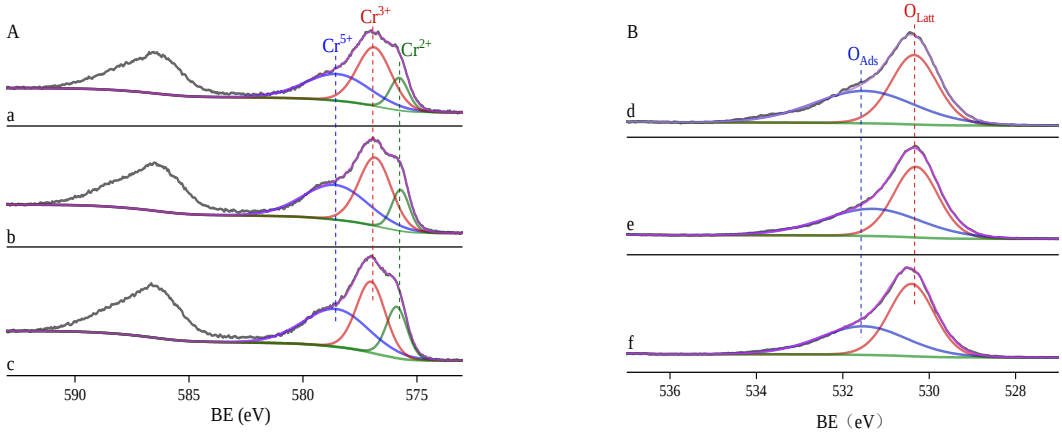

Figure 6. (**A**) Cr 2p (a) 0.4%CqM (b) 0.5%CqM (c) 0.6%CqM; (**B**) O 1s (d) 0.4%CqM (e) 0.5%CqM (f) 0.6%CqM.

Table 2. The binding energies of core electrons of xCqM and the percent of differential valence state.

XPS Spectra	Element Valence	0.4%CqM		0.5%CqM		0.6%CqM	
		Binding Energies, eV	Percent of Valence State, %	Binding Energies, eV	Percent of Valence State, %	Binding Energies, eV	Percent of Valence State, %
Cr 2p	Cr^{2+}	575.77	13.95	575.71	13.99	575.92	19.17
	Cr^{3+}	576.87	46.14	576.83	42.71	577.05	36.84
	Cr^{5+}	578.48	39.91	578.58	43.30	578.55	43.99
O 1s	O_{Latt}	530.35	49.47	530.30	54.40	530.41	56.73
	O_{Ads}	531.50	50.53	531.30	45.60	531.37	43.27

The O 1s spectrum (Figure 6B) could be fitted by two peaks, corresponding to lattice oxygen at 530.3–530.5 eV, and chemisorbed oxygen at 531.3–531.5 eV [59,60]. As the Ce content increases, the lattice oxygen content increases. The lattice oxygen ratio arrives at 56.73% when the Ce content is 0.6%. The conversion between Ce^{3+} and Ce^{4+} could create a charge imbalance and the vacancies [61]. The surfaces of the nanosized ceria particles encapsulated inside the quasi-MIL-101(Cr) pore will give rise to oxygen vacancies that promote the adsorption and activation of oxygen.

2.2. Catalytic Performance

2.2.1. NH_3-SCR Performance

NO_x conversions are displayed in Figure 7 for the quasi-MIL-101(Cr) and $xCeO_2$/quasi-MIL-101 catalysts at low temperatures. All of the catalysts exhibit good catalytic activities at a temperature window ranging from 175 °C to 300 °C, and they fall after 300 °C. In particular, the conversion of NO_x can be attained by 90% at 200 °C when $xCeO_2$/quasi-MIL-101 is used as a catalyst. This fact fully demonstrates that the catalytic activity of $xCeO_2$/quasi-MIL-101 is better than that of quasi-MIL-101(Cr) at low temperatures (<300 °C).

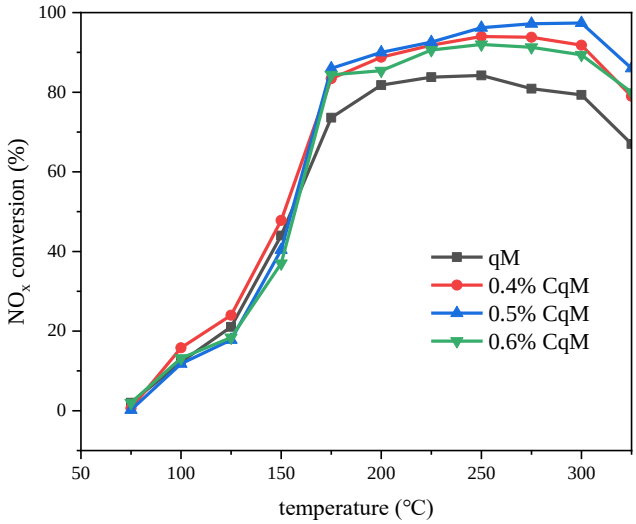

Figure 7. NO_x conversions over various catalysts. Reaction condition: [NH_3] = 500 ppm, [NO] = 500 ppm, [O_2] = 4%, and N_2 balance, the gas hourly space velocity (GHSV) = 79,000 h^{-1}.

Meanwhile, the catalyst has the best catalytic activity when the Ce content is 0.5%. Moreover, compared with the conventional Cr-Ce catalyst, the activation temperature of the $xCeO_2$/quasi-MIL-101 catalyst is improved. It can be shown by XPS that the increase of Ce content can improve the performance of Cr, which is caused by the electron conversion between Ce and Cr. However, the oxidation performance of CeO_2 is too high. As the content increases, the catalyst has undergone peroxidation to significantly change catalyst skeleton, which can be observed by XRD and FT-IR. At the same time, the NO_x conversion and the selectivity of N_2 decrease. The NO_x conversion rates of various catalysts are arranged in the following order: 0.5%CeO_2/quasi-MIL-101 > 0.4%CeO_2/quasi-MIL-101 > 0.6%CeO_2/quasi-MIL-101 > quasi-MIL-101(Cr). Panagintis et al. [62] explored the low-temperature selective catalytic reduction of NO_x with NH_3 by using Cr_xO_y supported on TiO_2. The results showed that the NO_x conversion rate could reach 90% at low temperature (120 °C), and the low-temperature activity of the catalyst we prepared failed to reach the expectation. However, compared with the Ti_xCr_yO catalyst prepared by Sounak Roy [63] et al. and the Cr/TiO_2 catalyst prepared by Bo Li [64] et al., the activity at the same temperature (>240 °C) was significantly better than that of both. Through the above analysis, it can be concluded that this material has basic catalytic performance, which is improved compared with the traditional Cr-based catalyst, but still does not reach the ideal low-temperature removal rate, which also provides a direction for the subsequent research of this kind of materials.

Figure 8 shows the selectivity of different catalysts for N_2 during the SCR reaction. As the temperature increases, the selectivity of all catalysts decreases to various extents. Compared with the quasi-MIL-101(Cr) catalyst, the $xCeO_2$/quasi-MIL-101 catalysts have higher N_2 selectivity. Among them, the catalyst with 0.5% Ce has the best selectivity to N_2. Similarly, excessive addition of Ce leads to the peroxidation of catalysts and decreases the selectivity to N_2. The most intuitive performance is the transformation of the catalyst skeleton, which can be observed by FT-IR and TEM.

Overall, both the SCR activity and N_2 selectivity of the catalyst with 0.5% Ce content are the best, which is attributed to the oxidizing ability of cerium oxide and the electron transfer between Cr and Ce. In addition, the peroxidation of 0.5% Ce content is too weak to ensure the efficiency of the NO_x conversion to N_2. The above data indicate that the 0.5%CeO_2/quasi-MIL-101 catalyst is relatively successful.

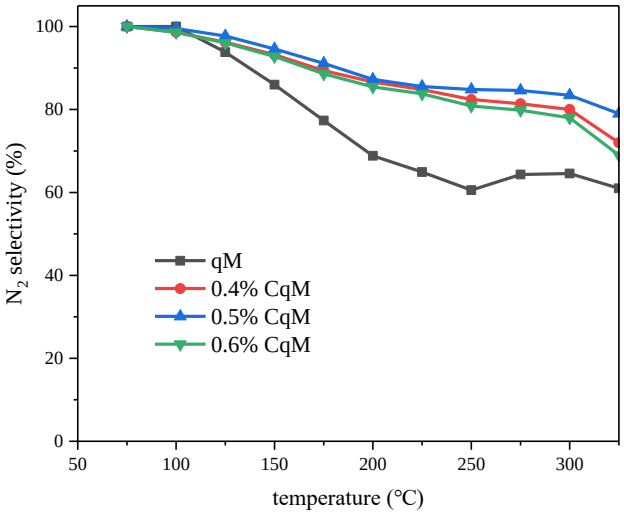

Figure 8. N_2 selectivity over various catalysts.

2.2.2. Effect of SO_2 and H_2O on the SCR Reaction

The SO_2 and H_2O in the flue gas impact the activity of the SCR catalyst significantly. The test results of the stability of the 0.5%CeO_2/quasi-MIL-101 catalyst under the conditions of 100 ppm SO_2 and 5% H_2O at 250 °C are shown in Figure 9.

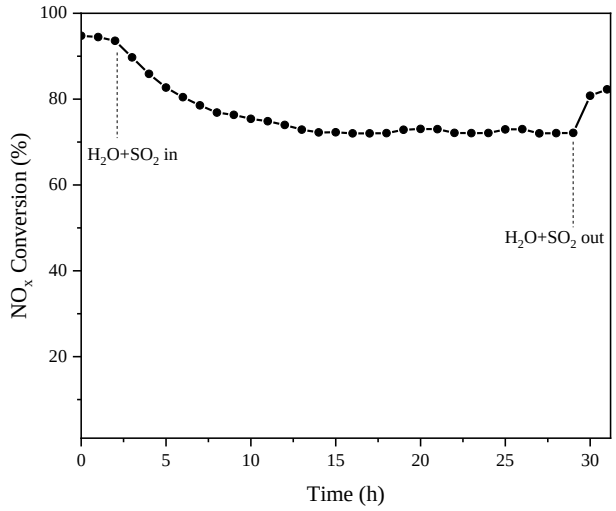

Figure 9. Stability test of the 0.5%CeO_2/quasi-MIL-101 catalyst in the presence of SO_2 and H_2O at 250 °C. Reaction conditions: 500 ppm NO, 500 ppm NH_3, 5% O_2, 5% H_2O and 100 ppm SO_2, balance N_2, GHSV = 79,000 h^{-1}.

Figure 9 indicates that the 0.5%CeO_2/quasi-MIL-101 catalyst has a high catalytic activity for NO_x at 250 °C during the SCR reaction without the introduction of SO_2 and H_2O. When 100 ppm SO_2 and 5% H_2O are introduced, the activity of the catalyst is affected, and the NO_x conversion rate was gradually stabilized after dropping to 70%. It could be attributed to two aspects: firstly, the competitive adsorption between reactants and SO_2 leads to the formation and deposition of sulfate on the surface of the catalyst, which inhibits the catalyst activity. Secondly, the competing adsorption between H_2O and NH_3/NO on the acid sites results in the occupation of the partial active sites on the catalyst surface by H_2O, which reduces the adsorption of reactive gases and makes catalyst poisoning inactivation. The precious literature has proved that Cr has excellent resistance to SO_2 and H_2O, compared with other metals, such as Mn, Co [52]. The NO_x conversion can be gradually restored to 80% after terminating

the introduction of SO_2 and H_2O. The above results indicate that the 0.5%CeO_2/quasi-MIL-101 catalyst also has good H_2O and SO_2 durability.

3. Experimental

3.1. Materials

Chromic nitrate nonahydrate [$Cr(NO)_3{\cdot}9H_2O$], terephthalate [H_2BDC], deionized water [H_2O], sodium hydroxide solution [NaOH], *N*,*N*-dimethylformamide [DMF], ethanol solution [C_2H_5OH] and n-hexane solution [C_6H_{14}].

3.2. Preparation of Catalysts

Preparation of MIL-101(Cr): MIL-101(Cr) was synthesized by the hydrothermal method, a mixture consisting of chromic nitrate nonahydrate ($Cr(NO)_3{\cdot}9H_2O$) and pure terephthalic acid (PTA, H_2BDC) were dissolved into H_2O (molar ratio = 1:1:277) with magnetic stirring, the NaOH solution (4 moL/L) was slowly added with the as-prepared solution to adjust the pH from 1.3 to 2.5. Then the mixtures were transferred into a 100 mL Teflon-lined autoclave, which was sealed and maintained at 200 °C for 24 h. After hydrothermal processing, the obtained samples were collected. The samples were respectively purified with *N*,*N*-dimethylformamide (DMF), and ethanol solution at 60 °C for 3 h to remove impurities, and finally, the filtered material was dried in a vacuum oven at 150 °C to obtain a green powder material.

Preparation of quasi-MIL-101(Cr): The thermal transformation of as-prepared purified MIL-101(Cr) materials were uniformly dispersed in a porcelain boat, placed in a muffle furnace, heated to 300 °C for 2 h, and cooled to room temperature to obtain a desired quasi-MOF material. For convenience, the resulting samples were labeled as quasi-MIL-101(Cr) materials, denoted as qM.

Preparation of xCeO_2/quasi-MIL-101(Cr): By a double-solvent method, MIL-101(Cr) materials were placed in an n-hexane solution by ultrasonication for 1 h, and to make it uniformly dispersed. Different concentrations of Ce^{3+} solution (x = 0.4%, 0.5%, 0.6%) prepared by dissolving Ce $(NO)_3{\cdot}6H_2O$ in deionized water, were added to the mixture solution by vigorous stirring at room temperature for 3 h. The samples were dried at 200 °C for 12 h and calcined 300 °C for 2 h in a muffle furnace. For convenience, the resulting samples were labeled as xCeO_2/quasi-MIL-101(Cr) materials, denoted as xCqM.

3.3. Catalyst Characterization

XRD patterns were obtained by using a Rigaku SmartLab Auto X-ray diffractometer (Tokyo, Japan) with Cu Kα radiation (λ = 1.5418 Å) in the 2–80° range. N_2 adsorption-desorption isotherms were measured at a liquid nitrogen temperature, using a micromeritics ASAP 2460 instrument (Micromeritics, Norcross, GA, USA) in static mode. Before the measurement, the catalysts were degassed at 300 °C for 4 h. The specific surface area was calculated by the BET equation, and pore volumes and average pore diameters were determined by using the Barrett–Joyner–Halenda (BJH) method from the desorption branch of the N_2 adsorption isotherm. An inductively coupled plasma optical emission spectrometer (ICPOES, Optima 2000DV) (Shanghai, China) was employed to determine the overall Ce content in the prepared catalyst. The morphologies of the catalysts and the structure of nano-ceria encapsulated inside quasi-MIL-101(Cr) were observed by SEM (XL-30 FEG Hillsboro, FEI Inc., Hillsboro, OR, USA) and TEM (TECNAI F20 Hillsboro, FEI Company, Hillsboro, OR, USA). The elemental distribution over the selected region was acquired by an energy dispersive X-ray spectrometer (EDS) attached to the transmission electron microscope (TEM). XPS measurements were carried out by a Thermo Fisher Scientific EscaLab 250Xi Electron Spectrometer (Shanghai, China) with monochromatic Al Kα radiation. The C 1s line at 284.6 eV was considered as a reference for the binding energy calibration. TG analysis was conducted by a thermogravimetric analyzer (Seiko TG/DTA 6300 Tokyo, Japan) under the condition of the air, which is at a heating rate of 5 °C/min from 37 °C to 600 °C. The FT-IR spectrum

was recorded on an FT-IR spectrometer (Bruker VERTEX 70-FT-IR Shanghai, China) with a standard KBr pellet method. All spectra were collected over accumulative 20 scans with a resolution of 8 cm^{-1} in the range of 3500–400 cm^{-1}.

3.4. Catalytic Activity Measurement

The NH_3-SCR activity measurement was carried out in a fixed-bed quartz rector (inner diameter 9 mm) loaded with approximately 0.12 g catalyst of 40–60 mesh. The typical composition of the reactant gas was as follows: 500 ppm NO, 500 ppm NH_3, 5% O_2 and N_2 as the balance gas. The total gas flow rate was 300 mL/min (atmospheric pressure), which corresponded to a gas hourly space velocity (GHSV) of 79,000 h^{-1}. The catalytic activity of the prepared catalysts was evaluated from 50 °C to 325 °C, and the concentrations of the NO, NO_2, and O_2 in the inlet and outlet streams were continually monitored by the FT-IR spectrometer (MKS6030HS). The NO_x conversion and the selectivity to N_2 were calculated according to the following equations:

$$NO_X \text{ conversion} = \frac{[NO_X]_{in} - [NO_X]_{out}}{[NO_X]_{in}} \times 100\%$$

$$N_2 \text{ selectivity} = \frac{[NO_X]_{in} + [NH_3]_{in} - [NO_X]_{out} - [NH_3]_{out} - 2[N_2O]_{out}}{[NO_X]_{in} + [NH_3]_{in} - [NO_X]_{out} - [NH_3]_{out}} \times 100\%$$

where $[NO_x] = [NO] + [NO_2]$, and $[NO_x]_{in}$ and $[NO_x]_{out}$ indicated the concentrations of NO_x at the inlet and outlet of the reactor at steady state, respectively.

4. Conclusions

In summary, ceria nanoparticles are successfully encapsulated within MIL-101(Cr) by a double-solvent method to prepare $xCeO_2$/quasi-MIL-101 with various Ce content. The $xCeO_2$/quasi-MIL-101 catalysts are enhanced NH_3-SCR activity at low temperatures. The 0.5%CeO_2/quasi-MIL-101 composite exhibits the fine catalytic activity at low temperature (<300 °C) with 98% NO_x conversion obtained at 275 °C, which is attributed to high dispersion of Cr and the strong electronic interaction between Ce and unsaturated Cr-O bond in quasi-MIL-101(Cr) to promote electron transfer between the active component and the cocatalyst. The research results verify that the introduction of Ce can effectively improve the catalytic performance of the catalyst at low temperatures. The composite catalysts display the good catalytic performance at low temperature by adjusting the loading content. This has laid a foundation for the doping of other metals, the change of material structure and the improvement of preparation methods, and provided favorable evidence for subsequent studies. It is expected that denitrification catalysts with excellent performance will be prepared at low temperatures in the future.

Supplementary Materials: The following are available online at http://www.mdpi.com/2073-4344/10/1/140/s1, Figure S1: TGA under air (5 °C/min heated rate) of $xCeO_2$/quasi-MIL-101, Figure S2: The diffraction peak of MIL-101(Cr) and MIL-101(Cr) samples of the published literature, Figure S3: Nitrogen adsorption-desorption isotherms of MIL-101(Cr), quasi-MIL-101(Cr) and $xCeO_2$/quasi-MIL samples, Figure S4: The SEM image of the MIL-101(Cr), Figure S5: (a) TEM image of 0.4% CeO_2/quasi-MIL-101 (b) TEM image of 0.5% CeO_2/quasi-MIL-101 (c) TEM image of 0.6% CeO_2/quasi-MIL-101.

Author Contributions: Conceptualization and methodology—H.H. and M.L.; formal analysis, investigation and data curation—H.H., W.W. and X.G.; writing—original draft preparation—H.H.; writing—review and editing—M.L., C.W., H.H., W.W. and G.-S.W. All authors have read and agreed to the published version of the manuscript.

Funding: This project was supported financially by the National Natural Science Foundation of China (no. 51672040 and 51672013), Science and Technology Research Projects of the Education Department of Jilin Province (no. JJKH20180429KJ) and Jilin City Science and Technology Bureau (no. 201750228).

Conflicts of Interest: The authors declare no conflict of interest.

References

1. Liu, Z.; Ihl Woo, S. Recent Advances in Catalytic DeNO$_x$ Science and Technology. *Catal. Rev.* **2006**, *48*, 43–89. [CrossRef]
2. Zhang, J.; Liu, F.; Liang, J.; Yu, H.; Liu, W.; Wang, X.; Peng, H.; Wu, P. Exploring the nano-size effect of mordenite zeolites on their performance in the removal of NO$_x$. *Ind. Eng. Chem. Res.* **2019**, *58*, 8625–8635.
3. Zhang, L.; Wen, X.; Lei, Z.; Gao, L.; Sha, X.L.; Ma, Z.H.; He, H.B.; Wang, Y.S.; Jia, Y.; Li, Y.H. Study on the mechanism of a manganese-based catalyst for catalytic, NO$_X$ flue gas denitration. *Aip Adv.* **2018**, *8*, 045004. [CrossRef]
4. Hueso, J.; Cotrino, J.; Caballero, A.; Espinos, J.; Gonzalezelipe, A. Plasma catalysis with perovskite-type catalysts for the removal of NO and CH_4 from combustion exhausts. *J. Catal.* **2007**, *247*, 288–297. [CrossRef]
5. Gholami, R.; Stere, C.E.; Goguet, A.; Hardacre, C. Non-thermal-plasma-activated de-NO$_x$ catalysis. *Philos. Trans. R. Soc. A Math. Phys. Eng. Sci.* **2018**, *376*, 20170054. [CrossRef] [PubMed]
6. Li, Y.; Cheng, H.; Li, D.; Qin, Y.; Xie, Y.; Wang, S. WO_3/CeO_2-ZrO_2, a promising catalyst for selective catalytic reduction (SCR) of NO$_x$ with NH_3 in diesel exhaust. *Chem. Commun.* **2008**, 1470–1472. [CrossRef]
7. Lai, J.-K.; Wachs, I.E. A Perspective on the Selective Catalytic Reduction (SCR) of NO with NH_3 by Supported V_2O_5–WO_3/TiO_2 Catalysts. *ACS Catal.* **2018**, *8*, 6537–6551. [CrossRef]
8. Zhu, M.; Lai, J.-K.; Tumuluri, U.; Ford, M.E.; Wu, Z.; Wachs, I.E. Reaction Pathways and Kinetics for Selective Catalytic Reduction (SCR) of Acidic NO$_x$ Emissions from Power Plants with NH_3. *ACS Catal.* **2017**, *7*, 8358–8361. [CrossRef]
9. Yang, R.G.; Han, L.; Yang, T. Research progress on new technology of denitrification in coal-fired power plants. *J. Northeast Electr. Power Univ.* **2010**, *30*, 17–20.
10. Locci, C.; Vervisch, L.; Farcy, B.; Domingo, P.; Perret, N. Selective Non-catalytic Reduction (SNCR) of Nitrogen Oxide Emissions: A Perspective from Numerical Modeling. *Flow Turbul. Combust.* **2017**, *100*, 301–340. [CrossRef]
11. Wang, Y.L.; Li, N.; Zhang, H.Z.; Cui, S.P.; Zhang, Y.N. Effect of the Cement Raw Meal Rate Value on SNCR deNO$_x$ Efficiency with NH_3 as Reducing Agent. *Mater. Sci. Forum* **2019**, *944*, 1215–1220. [CrossRef]
12. Wu, R.; Zhang, N.; Liu, X.; Li, L.; Song, L.; Qiu, W.; He, H. The Keggin Structure: An Important Factor in Governing NH_3–SCR Activity Over the V_2O_5–MoO_3/TiO_2 Catalyst. *Catal. Lett.* **2018**, *148*, 1228–1235. [CrossRef]
13. Xu, L.; Wang, C.; Chang, H.; Wu, Q.; Zhang, T.; Li, J. New Insight into SO_2 Poisoning and Regeneration of CeO_2-WO_3/TiO_2 and V_2O_5-WO_3/TiO_2 Catalysts for Low-Temperature NH_3-SCR. *Environ. Sci. Technol.* **2018**, *52*, 7064–7071. [CrossRef] [PubMed]
14. Shi, Y.F.; Chen, Y.; Zhang, Y.W.; Zhang, Q. Study on Denitration Performance of Fly Ash Supported Vanadium Oxide Low Temperature SCR Catalyst. *J. Northeast Electr. Power Univ.* **2015**, *35*, 59–63.
15. Gao, X.; Jiang, Y.; Fu, Y.; Zhong, Y.; Luo, Z.; Cen, K. Preparation and characterization of CeO_2/TiO_2 catalysts for selective catalytic reduction of NO with NH_3. *Catal. Commun.* **2010**, *11*, 465–469. [CrossRef]
16. Chen, Z.; Yang, Q.; Li, H.; Li, X.; Wang, L.; Chi Tsang, S. Cr–MnO$_x$ mixed-oxide catalysts for selective catalytic reduction of NO$_x$ with NH_3 at low temperature. *J. Catal.* **2010**, *276*, 56–65. [CrossRef]
17. Arfaoui, J.; Ghorbel, A.; Petitto, C.; Delahay, G. Withdrawn: Novel Vanadium supported onto mixed Molybdenum-Titanium Pillared Clay catalysts for the low temperature SCR-NO by NH_3. *Chem. Eng. J.* **2017**, *356*, 598–608. [CrossRef]
18. Qu, L.; Li, C.; Zeng, G.; Zhang, M.; Fu, M.; Ma, J.; Zhan, F.; Luo, D. Support modification for improving the performance of MnO$_x$–CeO_y/γ-Al_2O_3 in selective catalytic reduction of NO by NH_3. *Chem. Eng. J.* **2014**, *242*, 76–85. [CrossRef]
19. Selleri, T.; Gramigni, F.; Nova, I.; Tronconi, E. NO oxidation on Fe- and Cu-zeolites mixed with BaO/Al_2O_3: Free oxidation regime and relevance for the NH_3-SCR chemistry at low temperature. *Appl. Catal. B Environ.* **2018**, *225*, 324–331. [CrossRef]
20. Liu, J.; Guo, R.-T.; Li, M.-Y.; Sun, P.; Liu, S.-M.; Pan, W.-G.; Liu, S.-W.; Sun, X. Enhancement of the SO_2 resistance of Mn/TiO_2 SCR catalyst by Eu modification: A mechanism study. *Fuel* **2018**, *223*, 385–393. [CrossRef]
21. Cao, L.; Wu, X.; Xu, Y.; Lin, Q.; Hu, J.; Chen, Y.; Ran, R.; Weng, D. Ceria-modified WO_3-TiO_2-SiO_2 monolithic catalyst for high-temperature NH_3-SCR. *Catal. Commun.* **2019**, *120*, 55–58. [CrossRef]

22. Zhou, H.; Ge, M.; Wu, S.; Ye, B.; Su, Y. Iron based monolithic catalysts supported on Al_2O_3, SiO_2, and TiO_2: A comparison for NO reduction with propane. *Fuel* **2018**, *220*, 330–338. [CrossRef]
23. Ren, S.; Li, S.; Su, Z.; Yang, J.; Long, H.; Kong, M.; Yang, J.; Cai, Z. Poisoning effects of KCl and As_2O_3 on selective catalytic reduction of NO with NH_3 over Mn-Ce/AC catalysts at low temperature. *Chem. Eng. J.* **2018**, *351*, 540–547. [CrossRef]
24. Hou, Y.; Li, Y.; Li, Q.; Liu, Y.; Huang, Z. Insight into the role of TiO_2 modified activated carbon fibers for the enhanced performance in low-temperature NH_3-SCR. *Fuel* **2019**, *245*, 554–562. [CrossRef]
25. Shi, J.; Zhang, Y.; Fan, Z.; Chen, M.; Zhang, Z.; Shangguan, W. Widened Active Temperature Window of a Fe-ZSM-5 Catalyst by an Impregnation Solvent for NH_3-SCR of NO. *Ind. Eng. Chem. Res.* **2018**, *57*, 13703–13712. [CrossRef]
26. Yu, R.; Zhao, Z.; Shi, C.; Zhang, W. Insight into the Synergic Effect of Fe-SSZ-13 Zeolite and $FeMnTiZrO_x$ Catalyst with Enhanced Reactivity in NH_3-SCR of NO_x. *J. Phys. Chem. C* **2019**, *123*, 2216–2227. [CrossRef]
27. Zhu, L.; Liu, X.Q.; Jiang, H.L.; Sun, L.B. Metal-Organic Frameworks for Heterogeneous Basic Catalysis. *Chem. Rev.* **2017**, *117*, 8129–8176. [CrossRef]
28. Tang, J.; Yamauchi, Y. Carbon materials: MOF morphologies in control. *Nat. Chem.* **2016**, *8*, 638–639. [CrossRef]
29. Shekhah, O.; Liu, J.; Fischer, R.A.; Woll, C. MOF thin films: Existing and future applications. *Chem. Soc. Rev.* **2011**, *40*, 1081–1106. [CrossRef]
30. Damasceno Borges, D.; Normand, P.; Permiakova, A.; Babarao, R.; Heymans, N.; Galvao, D.S.; Serre, C.; De Weireld, G.; Maurin, G. Gas Adsorption and Separation by the Al-Based Metal-Organic Framework MIL-160. *J. Phys. Chem. C* **2017**, *121*, 26822–26832. [CrossRef]
31. Alezi, D.; Belmabkhout, Y.; Suyetin, M.; Bhatt, P.M.; Weselinski, L.J.; Solovyeva, V.; Adil, K.; Spanopoulos, I.; Trikalitis, P.N.; Emwas, A.H.; et al. MOF Crystal Chemistry Paving the Way to Gas Storage Needs: Aluminum-Based soc-MOF for CH_4, O_2, and CO_2 Storage. *J. Am. Chem. Soc.* **2015**, *137*, 13308–13318. [CrossRef] [PubMed]
32. Zhang, C.; Sun, L.; Yan, Y.; Shi, H.; Wang, B.; Liang, Z.; Li, J. A novel photo- and hydrochromic europium metal-organic framework with good anion sensing properties. *J. Mater. Chem. C* **2017**, *5*, 8999–9004. [CrossRef]
33. Chen, D.-M.; Zhang, N.-N.; Liu, C.-S.; Du, M. Template-directed synthesis of a luminescent Tb-MOF material for highly selective Fe^{3+} and Al^{3+} ion detection and VOC vapor sensing. *J. Mater. Chem. C* **2017**, *5*, 2311–2317. [CrossRef]
34. Bhadra, M.; Sasmal, H.S.; Basu, A.; Midya, S.P.; Kandambeth, S.; Pachfule, P.; Balaraman, E.; Banerjee, R. Predesigned Metal-Anchored Building Block for In Situ Generation of Pd Nanoparticles in Porous Covalent Organic Framework: Application in Heterogeneous Tandem Catalysis. *ACS Appl. Mater. Interfaces* **2017**, *9*, 13785–13792. [CrossRef]
35. Dhakshinamoorthy, A.; Asiri, A.M.; Garcia, H. Metal-Organic Framework (MOF) Compounds: Photocatalysts for Redox Reactions and Solar Fuel Production. *Angew. Chem. Int. Ed. Engl.* **2016**, *55*, 5414–5445. [CrossRef]
36. Zhu, Q.L.; Xu, Q. Metal-organic framework composites. *Chem. Soc. Rev.* **2014**, *43*, 5468–5512. [CrossRef]
37. Sennu, P.; Aravindan, V.; Lee, Y.-S. High energy asymmetric supercapacitor with 1D@2D structured $NiCo_2O_4$@Co_3O_4 and jackfruit derived high surface area porous carbon. *J. Power Sources* **2016**, *306*, 248–257. [CrossRef]
38. Janiak, C.; Vieth, J.K. MOFs, MILs and more: Concepts, properties and applications for porous coordination networks (PCNs). *New J. Chem.* **2010**, *34*, 2366–2388. [CrossRef]
39. Tan, B.; Luo, Y.; Liang, X.; Wang, S.; Gao, X.; Zhang, Z.; Fang, Y. Mixed-Solvothermal Synthesis of MIL-101(Cr) and Its Water Adsorption/Desorption Performance. *Ind. Eng. Chem. Res.* **2019**, *58*, 2983–2990. [CrossRef]
40. Hupp, J.T.; Poeppelmeier, K.R. Chemistry. Better living through nanopore chemistry. *Science* **2005**, *309*, 2008–2009. [CrossRef]
41. Zhao, T.; Jeremias, F.; Boldog, I.; Nguyen, B.; Henninger, S.K.; Janiak, C. High-yield, fluoride-free and large-scale synthesis of MIL-101(Cr). *Dalton Trans.* **2015**, *44*, 16791–16801. [CrossRef] [PubMed]
42. Wang, P.; Zhao, H.; Sun, H.; Yu, H.; Chen, S.; Quan, X. Porous metal–organic framework MIL-100(Fe) as an efficient catalyst for the selective catalytic reduction of NO_x with NH_3. *RSC Adv.* **2014**, *4*, 48912–48919. [CrossRef]

43. Zhang, M.; Huang, B.; Jiang, H.; Chen, Y. Metal-organic framework loaded manganese oxides as efficient catalysts for low-temperature selective catalytic reduction of NO with NH_3. *Front. Chem. Sci. Eng.* **2017**, *11*, 594–602. [CrossRef]
44. Jiang, H.; Zhou, J.; Wang, C.; Li, Y.; Chen, Y.; Zhang, M. Effect of Cosolvent and Temperature on the Structures and Properties of Cu-MOF-74 in Low-temperature NH_3-SCR. *Ind. Eng. Chem. Res.* **2017**, *56*, 3542–3550. [CrossRef]
45. Jiang, H.; Wang, Q.; Wang, H.; Chen, Y.; Zhang, M. MOF-74 as an Efficient Catalyst for the Low-Temperature Selective Catalytic Reduction of NO_x with NH_3. *ACS Appl. Mater. Interfaces* **2016**, *8*, 26817–26826. [CrossRef]
46. Evans, J.D.; Sumby, C.J.; Doonan, C.J. Post-synthetic metalation of metal-organic frameworks. *Chem. Soc. Rev.* **2014**, *43*, 5933–5951. [CrossRef]
47. Tsumori, N.; Chen, L.; Wang, Q.; Zhu, Q.-L.; Kitta, M.; Xu, Q. Quasi-MOF: Exposing Inorganic Nodes to Guest Metal Nanoparticles for Drastically Enhanced Catalytic Activity. *Chem* **2018**, *4*, 845–856. [CrossRef]
48. Wang, P.; Sun, H.; Quan, X.; Chen, S. Enhanced catalytic activity over MIL-100(Fe) loaded ceria catalysts for the selective catalytic reduction of NO_x with NH_3 at low temperature. *J Hazard. Mater.* **2016**, *301*, 512–521. [CrossRef]
49. Xu, W.; Yu, Y.; Zhang, C.; He, H. Selective catalytic reduction of NO by NH_3 over a Ce/TiO_2 catalyst. *Catal. Commun.* **2008**, *9*, 1453–1457. [CrossRef]
50. Qiu, L.; Meng, J.; Pang, D.; Zhang, C.; Ouyang, F. Reaction and Characterization of Co and Ce Doped Mn/TiO_2 Catalysts for Low-Temperature SCR of NO with NH_3. *Catal. Lett.* **2015**, *145*, 1500–1509. [CrossRef]
51. Boningari, T.; Ettireddy, P.R.; Somogyvari, A.; Liu, Y.; Vorontsov, A.; McDonald, C.A.; Smirniotis, P.G. Influence of elevated surface texture hydrated titania on Ce-doped Mn/TiO_2 catalysts for the low-temperature SCR of NO_x under oxygen-rich conditions. *J. Catal.* **2015**, *325*, 145–155. [CrossRef]
52. Zhang, J.; Zhang, S.; Cai, W.; Zhong, Q. The characterization of CrCe-doped on TiO_2-pillared clay nanocomposites for NO oxidation and the promotion effect of CeO_x. *Appl. Surf. Sci.* **2013**, *268*, 535–540. [CrossRef]
53. Ferey, G. A Chromium Terephthalate-Based Solid with Unusually Large Pore Volumes and Surface Area. *Science* **2005**, *309*, 2040–2042. [CrossRef] [PubMed]
54. Geng, Y.; Shan, W.; Yang, S.; Liu, F. W-Modified Mn-Ti Mixed Oxide Catalyst for the Selective Catalytic Reduction of NO with NH_3. *Ind. Eng. Chem. Res.* **2018**, *57*, 9112–9119. [CrossRef]
55. Fan, Z.; Shi, J.W.; Gao, C.; Gao, G.; Wang, B.; Niu, C. Rationally Designed Porous MnO_x-FeO_x Nanoneedles for Low-Temperature Selective Catalytic Reduction of NO_x by NH_3. *ACS Appl. Mater. Interfaces* **2017**, *9*, 16117. [CrossRef]
56. Gao, G.; Shi, J.-W.; Liu, C.; Gao, C.; Fan, Z.; Niu, C. Mn/CeO_2 catalysts for SCR of NO_x with NH_3: Comparative study on the effect of supports on low-temperature catalytic activity. *Appl. Surf. Sci.* **2017**, *411*, 338–346. [CrossRef]
57. Jiang, D.; Fang, G.; Tong, Y.; Wu, X.; Wang, Y.; Hong, D.; Leng, W.; Liang, Z.; Tu, P.; Liu, L.; et al. Multifunctional Pd@UiO-66 Catalysts for Continuous Catalytic Upgrading of Ethanol to n-Butanol. *ACS Catal.* **2018**, *8*, 11973–11978. [CrossRef]
58. Russo, N.; Fino, D.; Saracco, G.; Specchia, V. Studies on the redox properties of chromite perovskite catalysts for soot combustion. *J. Catal.* **2005**, *229*, 459–469. [CrossRef]
59. Zhang, F.; Tian, G.; Wang, H.; Wang, H.; Zhang, C.; Cui, Y.; Huang, J.; Shu, Y. CeO_2/TiO_2 monolith catalyst for the selective catalytic reduction of NO_x with NH_3: Influence of H_2O and SO_2. *Chem. Res. Chin. Univ.* **2016**, *32*, 461–467. [CrossRef]
60. Yang, R.; Huang, H.; Chen, Y.; Zhang, X.; Lu, H. Performance of Cr-doped vanadia/titania catalysts for low-temperature selective catalytic reduction of NO_x with NH_3. *Chin. J. Catal.* **2015**, *36*, 1256–1262. [CrossRef]
61. Campbell, C.T.; Peden, C.H. Chemistry: Oxygen Vacancies and Catalysis on Ceria Surfaces. *Science* **2005**, *309*, 713–714. [CrossRef] [PubMed]
62. Smirniotis, P.G.; Peña, D.A.; Uphade, B.S. Low-Temperature Selective Catalytic Reduction (SCR) of NO with NH_3 by Using Mn, Cr, and Cu Oxides Supported on Hombikat TiO_2. *Chembiochem.* **2010**, *32*, 2479–2482. [CrossRef]

63. Roy, S.; Hegde, M.S.; Madras, G. Catalysis for NO_x abatement. *Appl. Energy* **2009**, *86*, 2283–2297. [CrossRef]
64. Li, B.; Xiong, S.; Liao, Y.; Xiao, X.; Huang, N.; Geng, Y.; Zou, S.; Yang, S. Why the Low Temperature SCR Performance of Cr/TiO_2 Much Less than That of Mn/TiO_2: A Mechanism Study. *J. Phys. Chem. C* **2016**, *120*, 23511–23522. [CrossRef]